Clcn7$^{F318L/+}$ as a new mouse model of Albers-Schönberg disease

Caetano-Lopes J[1,2], Lessard SG[1,2], Hann S[1,2], Espinoza K[3], Kang KS[4], Lim KE[4], Horan DJ[4], Noonan HR[5], Hu D[6], Baron R[6], Robling AG[4], Warman ML[1,2,3].

1. Orthopaedic Research Laboratories, Boston Children's Hospital, Boston, MA, USA.

2. Department of Genetics, Harvard Medical School, Boston, MA, USA.

3. Howard Hughes Medical Institute, Boston Children's Hospital, Boston, MA, USA.

4. Department of Anatomy and Cell Biology, Indiana University School of Medicine, Indianapolis, IN, USA.

5. BBS Program, Harvard Medical School, Boston, MA, USA.

6. Division of Bone and Mineral Research, Harvard School of Dental Medicine, Boston, Massachusetts, USA.

Corresponding author:

Matthew L. Warman

Boston Children's Hospital

Orthopaedic Research Laboratories

Enders 250

320 Longwood Ave

Boston, MA, 02115

(617) 919-2371

email: matthew.warman@childrens.harvard.edu

This is the author's manuscript of the article published in final edited form as:

Caetano-Lopes, J., Lessard, S. G., Hann, S., Espinoza, K., Kang, K. S., Lim, K. E., … Warman, M. L. (2017). Clcn7F318L/+ as a new mouse model of Albers-Schönberg disease. Bone. https://doi.org/10.1016/j.bone.2017.09.007

Abstract

Dominant negative mutations in *CLCN7*, which encodes a homodimeric chloride channel needed for matrix acidification by osteoclasts, cause Albers-Schönberg disease (also known as autosomal dominant osteopetrosis type 2). More than 25 different *CLCN7* mutations have been identified in patients affected with Albers-Schönberg disease, but only one mutation (*Clcn7*^{G213R}) has been introduced in mice to create an animal model of this disease. Here we describe a mouse with a different osteopetrosis-causing mutation (*Clcn7*^{F318L}). Compared to *Clcn7*$^{+/+}$ mice, 12-week-old *Clcn7*$^{F318L/+}$ mice have significantly increased trabecular bone volume, consistent with *Clcn7*^{F318L} acting as a dominant negative mutation. *Clcn7*$^{F318L/F318L}$ and *Clcn7*$^{F318L/G213R}$ mice die by 1 month of age and resemble *Clcn7* knockout mice, which indicate that p.F318L mutant protein is non-functional and p.F318L and p.G213R mutant proteins do not complement one another. Since it has been reported that treatment with interferon gamma (IFN-G) improves bone properties in *Clcn7*$^{G213R/+}$ mice, we treated *Clcn7*$^{F318L/+}$ mice with IFN-G and observed a decrease in osteoclast number and mineral apposition rate, but no overall improvement in bone properties. Our results suggest that the benefits of IFN-G therapy in patients with Albers-Schönberg disease may be mutation-specific.

Keywords

Osteopetrosis; Albers-Schönberg disease; osteoclast; interferon-gamma

1. Introduction

Osteopetrosis is a genetically heterogeneous disease characterized by defective bone resorption, increased bone density, and skeletal fragility. Several types of osteopetrosis have been described and most are autosomal recessive [1]. An autosomal dominant form of osteopetrosis, also known as Albers-Schönberg disease, occurs in ~ 1:20,000 persons [2, 3]. Symptoms and signs of Albers-Schönberg disease generally appear in childhood or adolescence, and there is wide phenotypic variability within and across families. The phenotype in persons with Albers-Schönberg disease can cause debilitating problems and worsen over time, and no beneficial pharmacological therapy is currently available [3-5].

Albers-Schönberg disease is caused by dominant negative (i.e., antimorphic) mutations in *CLCN7*, the gene encoding the homodimeric chloride channel 7 (CLC-7). This channel functions as a slow voltage-gated $2Cl^-/1H^+$ exchanger [6, 7], and gating depends on conformational changes that are communicated from one subunit to the other in the dimer [8]. In osteoclasts, CLC-7 dimers transport chloride ions into the resorption lacunae. Complete deficiency of CLC-7 causes a severe form of autosomal recessive ostepetrosis by making osteoclasts unable to resorb bone. Heterozygous *CLCN7* mutations that produce a mutant protein, which interferes with the function of wildtype protein, cause Albers-Schönberg disease. More than 25 different heterozygous mutations that cause Albers-Schönberg disease have been identified [9].

In 2014, Alam *et al* [10] described mice with a *Clcn7* knockin allele ($Clcn7^{G213R}$), which is the most common mutation reported in patients with Albers-Schönberg disease [11]. Mice homozygous for $Clcn7^{G213R}$ had a severe osteopetrotic phenotype and died weeks after birth, whereas heterozygous mice (i.e., $Clcn7^{G213R/+}$) had a phenotype that resembled Albers-Schönberg disease, including increased areal BMD, increased BV/TV, and increased osteoclast numbers with reduced activity [10]. When the mutant allele was crossed into

different genetic backgrounds, the highest percent increase in BV/TV compared to controls was found with the 129S1 background, followed by DBA/D2, C57BL/6J and Balb/c backgrounds [12]. Since interferon gamma (IFN-G) has been reported to benefit some patients with recessive forms of osteopetrosis [13], this therapy was evaluated in *Clcn7*$^{G213R/+}$ mice. Thrice weekly IFN-G injection in *Clcn7*$^{G213R/+}$ mice on the 129S1 background, from 4 to 12 weeks of age, significantly reduced trabecular bone BV/TV; one reason for this improvement seemed to be improved osteoclast function as indicated by increase in the serum CTX/TRAPc5b ratio [14].

We created mice with a different osteopetrosis-associated *Clcn7* knockin mutation (*Clcn7*^{F318L}). Here we describe the phenotype of mice with *Clcn7*^{F318L} alleles and their response to IFN-G therapy.

2. Methods

The Institutional Animal Care and Use Committee at Boston Children's Hospital approved this work. All experiments were conducted in accordance with the National Institutes of Health guide for the care and use of Laboratory animals (NIH Publications No. 8023, revised 1978).

2.1 Creation of mice with a *Clcn7*^{F318L} knockin allele

A 779-basepair fragment containing coding exon 11 of *Clcn7* was PCR amplified using JM8A3.N1 mouse embryonic stem (ES) cell [15] genomic DNA as template. The amplimer was subcloned into pBluescript II KS+ (pBSII KS+) and a p.F318L missense mutation was introduced by site directed mutagenesis (Agilent Technologies, CA, USA). Note the actual mouse mutation is p.F316L, but we use the human protein nomenclature when referring to this allele throughout this manuscript. Using the same stem cell genomic DNA as template,

4.5 kb upstream and 2.5 kb downstream targeting arms were PCR amplified (5' arm: P1- AGAGTTTCTCTGTGTAGCCATTGTT, P2- ACTGAAGAAAGCACAGTGAGCG; 3' arm: P3- CCCTTAGGAACTTCGCATAGTTAGC, P4- CTGGAGTGGGTAGGACAT). The targeting arms along with the p.F318L mutation containing fragment, were combined by in-fusion cloning (Clontech, CA, USA) with a floxed neomycin selection cassette and a thymidine kinase selection cassette to produce the targeting vector depicted in Figure 1A. Homologous recombination of the linearized construct was performed in JM8A3.N1 ES cells [15] using ganciclovir and neomycin selection. Correctly targeted ES cells were identified by long-range PCR across both homology arms (5'end: P5- GAGCAGGAGTTACAGCTGGG, P6- GCTCGACTAGAGCTTGCGGA; 3'end: P7- CCACTTGTGTAGCGCCAAG; P8- TCCCCACACACCTACTGACA). A correctly targeted clone with a normal karyotype was introduced into C57BL/6J blastocysts to produce chimeric mice, which were then crossed to C57BL/6J mice to attain germline transmission of the p.F318L mutation. Tg(Gata1-cre)1Sho [16] mice were then used to Cre-excise the neomycin selection cassette. The final *Clcn7*^{F318L} allele used in these studies is depicted in Figure 1A.

2.2 Animal breeding, maintenance, and genotyping

Clcn7$^{F318L/+}$ mice were intercrossed, crossed with C57BL/6J mice, or crossed with *Clcn7*$^{G213R/+}$ mice [10]. Offspring were tail clipped at 10 days of age, weaned before 28 days of age and then housed with same-sex littermates. Tail snip DNA was recovered using the HotSHOT method [17]. For genotyping the *Clcn7*^{F318L} allele, PCR primers (P9: GCTCCTCAGACGCATGGAAT and P10: AGAAAACAGGAGAGCTGGCA), which generate a 407 bp amplimer for the wildtype allele and a 530 bp amplimer for the *Clcn7*^{F318L} allele (Figure 1B) were used. *Clcn7*^{G213R} genotyping was performed as previously described [10].

2.3 Phenotypic assessment

Twenty-one day old mice were sacrificed using CO_2 followed by cervical dislocation. Prior to sacrifice, animals were weighed and bone mineral density (BMD) was measured with the Piximus II dual energy X-ray absorptiometer (GE Lunar, Madison, WI). After sacrifice, femurs and 4th lumbar vertebra were removed, dissected free of soft tissue, and either placed in 4% paraformaldehyde (PFA) at room temperature for micro-computed tomography (μCT) and histomorphometry analysis or wrapped in saline soaked gauze and frozen at -20°C for biomechanical measurements.

Twelve-week-old mice, which had received intraperitoneal (IP) Calcein (Sigma, MO, USA; 10mg/Kg) when 11-weeks-old, and IP Alizarin complexone (Sigma, MO, USA; 20mg/Kg) when 11-weeks and 4-days old as previously described [18], were fasted for 6 hours prior to sacrifice. Prior to euthanasia by CO_2 and cervical dislocation, the animals were weighed and had their BMD measured. After euthanasia, cardiac puncture was performed to collect blood for serum markers of bone anabolism and catabolism. Femora and 4th lumbar vertebrae were removed and processed as described earlier.

2.4 IFN-G treatment

Wild type (i.e., *Clcn7*$^{+/+}$) and mutant (i.e., *Clcn7*$^{F318L/+}$ and/or *Clcn7*$^{F318L/F318L}$) mice were randomized to receive subcutaneous injection of vehicle (50 μl of 0.1% BSA in PBS) or recombinant mouse IFN-G (stock number 485-MI, R&D Systems, MN, USA; 37.5 μg/kg/dose of a 10 μg/ml stock solution). When therapy began at P10, injections were given 5 times/week until P22 (10 doses total). Mice were then sacrificed. When therapy began at 4 weeks of age, injections were given 3 times/week until 12 weeks of age. Mice were then sacrificed.

2.5 RT-PCR to assess splicing of the *Clcn7*^{F318L} allele

mRNA was recovered from *Clcn7*$^{+/+}$, *Clcn7*$^{F318L/+}$ and *Clcn7*$^{F318L/F318L}$ 3-week-old mouse tibiae after the bone marrow was removed. Reverse transcription cDNA synthesis was performed using 200 ng of RNA from each sample with the ProtoScript II First Strand cDNA Synthesis Kit (New England Biolabs, MA, USA), according to the manufacturer's instructions. Primers located in exons 5 and 13 were used to amplify *Clcn7* cDNA. (Forward primer: CCGCGTCATCAAGGACAACAT, reverse primer: TGGTGTAGGCCATTTTCTCTG). Amplimers were separated by gel electrophoresis to determine if splicing of the *Clcn7*^{F318L} allele was the same as that of the *Clcn7*$^{+}$ allele.

2.6 Droplet digital PCR to assess relative abundance of *Clcn7*^{F318L} mRNA in heterozygous mice

RNA was recovered from liver, kidney and marrow-free tibia of 3-week-old *Clcn7*$^{+/+}$, *Clcn7*$^{F318L/+}$, and *Clcn7*$^{F318L/F318L}$ mice and used to prepare cDNA as described above. A forward primer located in exon 10 and a reverse primer spanning the junction of exons 12 and 13 were used to amplify *Clcn7* transcript (ddPCR-F: AGCTGGTGTATCTGCTGCATT; ddPCR-R: TGGTGTAGGCCATTTTCTCG, 233bp). Fluorescent probes that distinguish *Clcn7*^{F318L} amplimer (56-FAM/AGAGGGCGCCTCCCTCTGGAATCA/3IABkFQ) from *Clcn7*$^{+}$ amplimer (5HEX/AAGAGGGCGCCTCCTTCTGGAATCAGT/3IABkFQ) were purchased (Integrated DNA Technologies, IA, USA). Prior to performing ddPCR, cDNA concentrations were adjusted to 10 ng/µl in water. Thirty ng of cDNA template was used per reaction with the BioRad Supermix for Probes protocol. Droplets were created on a BioRad automatic droplet generator and PCR (95°C/10mins; 94°C/30s; 60°C/60s; 72°C/20s; 40 cycles; 98°C/10mins – cycling ramp speed was set to 1.2°C/s) was performed on Eppendorf

ep gradient S machine thermocycler (Eppendorf, Germany). Droplets containing *Clcn7*$^{+}$ or *Clcn7*^{F318L} amplimers were counted on a BioRad QX200 sample reader and analysed with Quantasoft software (BioRad, CA, USA).

2.7 Immunofluorescence detection of CLC-7 protein

Long bones collected from P18 *Clcn7*$^{+/+}$ and *Clcn7*$^{F318L/F318L}$ mice were briefly cleaned in ethanol before their marrow cavities were flushed with Hank's Balanced Salt Solution (HBSS, Gibco, MA, USA) to collect bone marrow. Red blood cells in the bone marrow samples were lysed using RBC lysis buffer (Roche, IN, USA) and the remaining cells were plated in Dulbecco's Modified Eagle Medium (DMEM, Gibco, MA, USA) supplemented with 10% fetal bovine serum (FBS, Gibco, MA, USA), 100U/mL penicillin/streptomycin (Gibco, MA, USA) and 40ng/mL macrophage colony-stimulating factor (M-CSF, Peprotech, UK) on 6-well plates (Denville, MA, USA), and kept overnight in a cell culture incubator at 37°C in 5% CO_2. The following day, non-adherent cells were collected, centrifuged at 400 x g for 10 minutes, resuspended in 2 ml of DMEM, counted on a hemocytometer, and plated at 12,000 cells per chamber slide (Corning, NY, USA) in DMEM, with 10% FBS, 100U/mL penicillin/streptomycin, and 40ng/mL M-CSF for 2 additional days. Cells were then fixed in 4% PFA and incubated with rabbit anti-CLC-7 polyclonal antibody (stock number sc-28755, Santa Cruz Biotechnology, TX, USA; diluted 1:100 in PBS/BSA/Tween, which contains 1% BSA and 0.1% Tween20) for 1 hour at room temperature and then overnight at 4°C. After 3 x 10 minute washes in PBS/BSA/Tween, a FITC-labeled anti-rabbit IgG goat monoclonal antibody (stock number sc-2012, Santa Cruz Biotechnology, TX, USA; diluted 1:300 in PBS/BSA/Tween) was added to the chamber slide and incubated for 1 hour at room temperature. Slides that had only been incubated with FITC-labeled anti-rabbit IgG goat monoclonal antibody served as a negative control. After another 3 x 10 minute washes in

PBS/BSA/Tween the slides were air-dried, stained with Hoechst 33342 (LifeTechnologies, MA, USA) to visualize nuclei, and cover slipped. Fluorescence images were captured on a Nikon upright fluorescence microscope (Nikon, NY, USA) at a magnification of 400X.

2.8 BMD measurements

Whole body scanning was performed using a Piximus II dual energy X-ray absorptiometer (GE Lunar, Madison, WI) with 0.18mm x 0.18mm resolution. The machine was calibrated before each scanning session using a phantom supplied by the manufacturer. The scan was performed with the mice in a prone position under 2.5% isoflurane (Baxter, IL, USA) anesthesia, with each limb spread on a plastic tray. Measurements of BMD (g/cm^2) and bone mineral content (BMC, g) were obtained from the whole-body data after excluding the calvarium, mandible and teeth.

2.9 μCT measurements

Femoral midshaft cortical bone, distal femur trabecular bone, and 4^{th} lumbar vertebra were scanned on a Scanco μCT-35 specimen scanner (Scanco Medical AG, Switzerland) as previously described [19, 20]. Briefly, the tomography parameters used were as follows: 50 kV, 120 mA, 151-ms integration time, and 10-μm voxel resolution. Morphometric measures included trabecular bone volume fraction (BV/TV, %), trabecular number (Tb.N, 1/mm), trabecular thickness (Tb.Th, mm), trabecular separation (Tb.Sp, mm), trabecular bone mineral content (BMC, mgHA), cortical area fraction (Ct.Ar/Tt.Ar, %) and cortical thickness (Ct.Th, mm) [21].

2.10 Histomorphometry measurements

At the time of sacrifice, femurs were collected from 7-10 male 12-week-old *Clcn7*$^{+/+}$, *Clcn7*$^{F318L/+}$ and IFN-G treated *Clcn7*$^{F318L/+}$ mice for histomorphometric analysis. Osteoblast and osteoclast numbers and density, and dynamic bone formation parameters, were measured using standard procedures recommended by the American Society of Bone and Mineral Research (ASBMR) histomorphometry committee [22].

2.11 Three-point bending test

Femur biomechanical studies were performed as previously described [19, 20] using a TestResources 100 Series electromechanical test machine (TestResources, Inc., Shakopee, MN, USA) with a force resolution of 0.005N. Femoral diaphyses were loaded to failure in a three-point bending apparatus, using a cross-head speed of 0.2mm/s, during which force and displacement measurements were collected every 0.005s. Lower supports were positioned 8.2 mm apart. From the force-displacement curve, yield force (N), stiffness (N/mm), ultimate force (N) and energy to ultimate force (mJ) were calculated [19, 20].

2.12 Assays for anabolic and catabolic bone markers, and for IFN-G levels, in serum

Whole blood collected by cardiac puncture was placed in Serum Separator BD Microgard tubes (BD, Franklin Lakes, NJ), centrifuged at 1723 x g for 15 min at 4°C. The separated serum was recovered and stored at -80°C. Serum levels of collagen type I cross-linked C-telopeptide (CTX-I), tartrate-resistant acid phosphatase 5b isoform (TRAcP 5b) and procollagen type 1 N-terminal propeptide (P1NP) were measured by enzyme-linked immunosorbent assay (ELISA) according to the manufacturers' instructions (kit numbers AC-06F1, SB-TR103 and AC-33F1, respectively; Immunodiagnostics Systems, UK).

Ten 8-week-old female C57BL/6J mice were randomized to receive a single subcutaneous injection of either vehicle or mouse IFN-G (37.5 µg/kg). Two hours later the animals were

euthanized by CO_2, blood was collected by cardiac puncture, and serum separated as described above. Serum concentration of mouse IFN-G was measured using the Quantikine IFN-gamma ELISA kit (kit number MIF00; R&D Systems, MN, USA).

2.13 Statistical analyses

Statistical analyses were performed using SPSS Statistics 23.0 (IBM). Continuous variables were expressed as mean ± 1 standard deviation (±1SD). Multiple groups were compared using analysis of variance (ANOVA) test followed by Bonferroni's multiple comparison test. Statistical significance was considered when p-values were ≤ 0.05.

3. Results

3.1 The *Clcn7*^{F318L} allele acts as a loss-of-function allele when either homozygous or compound heterozygous with the *Clcn7*^{G213R} allele, and as a dominant negative allele when heterozygous with a *Clcn7*$^{+}$ allele.

Clcn7$^{F318L/+}$ mice are viable and fertile. When intercrossed, *Clcn7*$^{F318L/F318L}$ offspring are born at expected Mendelian frequencies, but die when ~ 1 month of age. Homozygous mutant offspring are runted and do not have tooth eruption, recapitulating the phenotype seen in mice with knockout alleles in *Clcn7* (i.e., *Clcn7*$^{-/-}$) that fail to produce protein [23]. Therefore, to determine whether the *Clcn7*^{F318L} knockin allele is capable of producing a mutant protein, we performed 3 different assays. First, we used RT-PCR with a primer-pair anchored 5 exons upstream of the intron with the residual loxP site and 2 exons downstream of the missense mutation containing exon to determine if the *Clcn7*^{F318L} allele is spliced normally. We observed the same sized RT-PCR product in wildtype, heterozygous, and homozygous mice, consistent with the knockin allele having normal mRNA splicing (Figure 1D). Second, we quantified the amount of wildtype and mutant transcript expressed in

heterozygous mice using droplet digital PCR. We observed equal numbers of wildtype and mutant transcripts in cDNA from bone (Figure 1E), kidney and liver (data not shown). Third, we used an anti-CLC-7 antibody to detect protein in cultured bone marrow cells. We observed similar immunofluorescence in cells from *Clcn7*$^{+/+}$ and *Clcn7*$^{F318L/F318L}$ mice (Figure 1F). Taken together, these data indicate that the *Clcn7*^{F318L} allele is normally expressed and translated into protein. Therefore, mutant protein is produced but is non-functional.

We next crossed *Clcn7*$^{F318L/+}$ mice with *Clcn7*$^{G213R/+}$ mice and generated compound heterozygous offspring to determine if the two mutant proteins could complement each other. *Clcn7*$^{F318L/G213R}$ mice lack tooth eruption, are runted, and die by ~ 1 month of age (data not shown), just like the *Clcn7*$^{F318L/F318L}$ mice. Therefore, there is no evidence of complementation.

We next turned our attention to *Clcn7*$^{F318L/+}$ mice. When examined at 12 weeks of age, we found a slight increase in BMD in males *Clcn7*$^{F318L/+}$ mice compared to *Clcn7*$^{+/+}$ mice. The most significant μCT differences we observed in male and female *Clcn7*$^{F318L/+}$ mice compared to *Clcn7*$^{+/+}$ mice were in trabecular bone (measured both in the femur (Figure 2) and vertebra (data not shown)). Only male *Clcn7*$^{F318L/+}$ mice showed differences for cortical bone parameters and three-point bending assays of bone strength when compared to *Clcn7*$^{+/+}$ mice (Figure 2).

3.2 Only *Clcn7*$^{F318L/F318L}$ and *Clcn7*$^{F318L/G213R}$ mice have obvious skeletal phenotypes at 3 weeks of age.

To determine whether it is possible to consistently observe effects of the *Clcn7*^{F318L} allele in younger animals, we performed DEXA, μCT and three-point bending tests on *Clcn7*$^{+/+}$, *Clcn7*$^{F318L/+}$ and *Clcn7*$^{F318L/F318L}$ mice at 3 weeks of age. *Clcn7*$^{F318L/F318L}$ mice were significantly smaller and had greater BMD than *Clcn7*$^{F318L/+}$ and *Clcn7*$^{+/+}$ mice, as measured

by DEXA ($p<0.05$, Figure 3). No significant differences were observed between 3-week-old *Clcn7*$^{F318L/+}$ and *Clcn7*$^{+/+}$ mice. Therefore, the effectiveness of any therapeutic intervention will not be detected by μCT in 3-week-old *Clcn7*$^{F318L/+}$ mice.

3.3 Interferon-gamma therapy did not reduce the trabecular bone volume in *Clcn7*$^{F318L/+}$ mice

It has previously been reported that IFN-G therapy benefitted some patients with autosomal recessive forms of osteopetrosis [13] as well as the *Clcn7*$^{G213R/+}$ mouse model of Albers-Schönberg disease [14]. IFN-G is only FDA approved for the treatment of autosomal recessive malignant osteopetrosis, but it may be used "off-label" in patients with Albers-Schönberg disease. Therefore, we treated *Clcn7*$^{F318L/+}$ mice from 4 to 12 weeks of age, using an agent and dosing schedule that improved skeletal properties and markers of bone turnover in *Clcn7*$^{G213R/+}$ mice [14]. We confirmed the bioavailability of IFN-G by measuring serum levels 2 hours after subcutaneous injection. Mice that received IFN-G had orders-of-magnitude fold-increases in serum levels compared to vehicle-treated mice ($p<0.0001$). As previously reported [14] for *Clcn7*$^{G213R/+}$ mice that received IFN-G, we also observed no adverse effects of IFN-G in *Clcn7*$^{F318L/+}$ mice. At the end of the experiment, the average weight of mice receiving IFN-G did not significantly differ from that of mice receiving vehicle (Figure 4). However, treatment with IFN-G was not associated with a change in tBMD or rabecular bone BV/TV (Figure 4).

We also administered IFN-G to *Clcn7*$^{F318L/F318L}$ mice beginning when they were 11 days of age. However, rather than benefitting these animals, we observed that these mice died before the protocol could be completed, whereas vehicle treated mice did not.

3.4 *Clcn7*$^{F318L/+}$ mice have increased osteoclast number, which is reduced by interferon-gamma therapy.

Histomorphometry, which was only performed in male mice, revealed more osteoclasts per bone perimeter and surface area in *Clcn7*$^{F318L/+}$ mice compared to *Clcn7*$^{+/+}$ mice. Consistent with this observation both *Clcn7*$^{F318L/+}$ male and female mice had increased serum TRAPc5b compared to *Clcn7*$^{+/+}$ littermates.

Decreased numbers of osteoclasts per bone perimeter and per surface area were observed, as was decreased serum TRAcP5b, in IFN-G treated *Clcn7*$^{F318L/+}$ mice compared to vehicle treated *Clcn7*$^{F318L/+}$ mice (Figure 5). However, the IFN-G effect on osteoclasts was not associated with a change in trabecular bone BV/TV (Figure 4), perhaps because IFN-G treatment also modestly lowered BFR/BV in *Clcn7*$^{F318L/+}$ mice (Figure 5).

4. Discussion

Here we describe a second mouse model of Albers-Schönberg disease. More than 25 different causal mutations have been identified in patients and *ex vivo* studies suggest that mutations may negatively impact CLC-7 channel function via different mechanisms [6]. Consequently, having more than one animal model makes it possible to ask whether an intervention that is beneficial for one mutation could have broad benefit.

The use of an allelic spectrum of disease-causing mutations when searching for disease-modifying drugs has already been demonstrated for other diseases, such as osteogenesis imperfecta [18, 24-30] and cystic fibrosis [31]. Six classes of mutations have been reported in the gene responsible for causing cystic fibrosis based on the effect of the mutation of protein synthesis, trafficking, and function [31]. In the case of cystic fibrosis, which is associated with thousands of different disease-causing mutations in CFTR, drugs that significantly help patients with one class of mutations may be ineffective in patients with other classes. Here,

we may have observed a similar difference in responsiveness to IFN-G between mice with different mutations in *Clcn7*.

The p.G213R allele has been detected in several different families with Albers-Schönberg disease [11], but the p.F318L allele is less common. Nevertheless, the *CLCN7* p.F318L mutation in humans is a *bona fide* osteopetrosis-causing mutation and the *Clcn7*^{F318L} allele in the mouse appears to recapitulate the human phenotype. Mutant (p.F318L) CLC-7 protein likely inhibits the function of wild-type CLC-7 as a heterodimer. Although we have not formally demonstrated this *in vitro* or *ex vivo*, we conclude this is the case since *Clcn7*$^{F318L/+}$ mice have significantly increased BV/TV, which is not observed in mice that are heterozygous for a *Clcn7* knockout (i.e., *Clcn7*$^{+/-}$) mutation [23].

Consistent with a previous report that used IFN-G in the *Clcn7*$^{G213R/+}$ mouse model [14] we found that IFN-G increased the CTX/TRAcP5b ratio, suggesting osteoclast function improves. Quantitative histomorphometry was not performed in the *Clcn7*$^{G213R/+}$ mouse IFN-G study, although an increase in osteoclast number was observed when this mouse model was first described and has also been reported in patients with Albers-Schönberg disease [10, 32]. Histomorphometric analyses in our *Clcn7*$^{F318L/+}$ mice also revealed an increased number of osteoclasts, that decreased in response to IFN-G treatment, consistent with the reduction in serum TRAcP5b levels. However, in contrast to *Clcn7*$^{G213R/+}$ mice, IFN-G did not increase CTX-I levels in *Clcn7*$^{F318L/+}$ mice, nor did it normalize BV/TV. Thus, the putative effect of IFN-G on osteoclast function in *Clcn7*$^{F318L/+}$ mice is lower than that in *Clcn7*$^{G213R/+}$ mice.

The difference in the effectiveness of IFN-G in *Clcn7*$^{F318L/+}$ versus *Clcn7*$^{G213R/+}$ mice may be explained by differences in how these two mutations impact CLC-7 trafficking and function. Cell transfection studies expressing mutant CLC-7 proteins indicate that some missense mutations cause retention of protein in the endoplasmic reticulum (ER) [6, 33], whereas other missense mutations do not affect localization but change channel activity [6].

Cells expressing the p.G213R mutant CLC-7, retain the mutant protein in the endoplasmic reticulum [6, 33]. In contrast, cells expressing p.F318L mutant CLC-7 can transport the mutant protein to the lysosomal membrane where it is unable to produce plasma membrane current, suggesting that this mutation interferes with ion transport but not protein trafficking [6]. Thus, if IFN-G worked by improving CLC-7 channel trafficking in osteoclasts, it could benefit *Clcn7*$^{+/+}$ and *Clcn7*$^{G213R/+}$ mice by allowing protein to reach the ruffled membrane more efficiently. In *Clcn7*$^{G213R/+}$ mice, this would reduce the retention of mutant protein in the ER. Since CLC-7 dimers in *Clcn7*$^{F318L/+}$ mice do not appear to have a trafficking problem, IFN-G therapy would not be expected to have the same degree of benefit in these animals.

IFN-G is a cytokine that plays a critical role in both innate and adaptive immune responses, and is produced by natural killer (NK), NK T cells, CD4 and CD8 cells [34]. In 1995 this drug showed some benefit in severe osteopetrosis patients [13] and, in a case report, benefit in a patient with intermediate osteopetrosis [35]. However, whether benefit derives from IFN-G actions on osteoclasts remains uncertain. *In vitro* studies showed that osteoclasts from patients with osteopetrosis stimulated with IFN-G were larger and had increased *TRAP* expression [36]. However, when this experiment was performed using control osteoclasts, IFN-G inhibited osteoclast formation and lowered Cathepsin K mRNA expression [37]. Adding to these puzzling results, IFN-G Receptor 1 knockout mice display an osteoporotic phenotype associated with reduced mineral apposition and bone formation but also reduced markers of osteoclast activity [38]. Moreover, exogenous administration of IFN-G in ovariectomized mice increased BMD and bone strength, rescuing the disease [39]. Thus, the IFN-G effect on bone is not restricted to osteoclasts. Histomorphometric analyses revealed an increased number of osteoclasts in *Clcn7*$^{F318L/+}$ mice compared to wildtype mice, as has been previously reported in the *Clcn7*$^{G213R/+}$ mice and in patients with Albers-Schönberg disease [10, 32]. In *Clcn7*$^{F318L/+}$ mice, IFN-G decreased osteoclast number, which is

consistent with the reduction in serum TRAcP5b levels we observed in treated mice. With respect to bone formation, *Clcn7*$^{F318L/+}$ mice were not significantly different from wildtype mice, similar to what has been reported for Albers-Schönberg disease [40]. Although IFN-G therapy increased the active mineralizing surface in *Clcn7*$^{F318L/+}$ mice, it decreased the mineral apposition rate. Overall there was no effect of IFN-G on bone formation, μCT measurements of BV/TV and the serum measurements of P1NP.

Having a second mouse model with a dominant negative mutation in *Clcn7* that impairs osteoclast function makes it possible in a pre-clinical model to understand how drugs that affect CLC-7 trafficking and/or function might affect bone properties in patients with Albers-Schönberg disease.

Author contributions

JCL, SH, and MLW design the study, JCL, SGL, KE, KSK, HRN, KEL, DJH and DH collected the data. JCL, SH, AGR and RB analyzed the data. JCL and MLW wrote the initial draft of the manuscript. All authors edited, revised, and approved this version of the manuscript.

Declaration of interest

The authors declare no competing financial interests.

Funding: This work was supported by a grant from the Ciongoli Family, by the Children's Orthopaedic Surgery Foundation and by the National Institutes of Health (grant number AR053237).

Acknowledgements

The authors thank Dr. Michael Econs for sharing the *Clcn7*$^{G213R/+}$ mice, Dr. Stuart Orkin for sharing the Tg(Gata1-cre)1Sho mice, Dr. Antonio Maurizi and Dr. Anna Teti for sharing technical expertise regarding immunodetection of CLC-7, Mr. Michael Marcotrigiano for help with obtaining BMD and BMC measurements, and the Gene Manipulation & Genome Editing Core, F.M. Kirby Neurobiology Center, Boston Children's Hospital for assistance in generating the *Clcn7*^{F318L} knockin mouse.

References

[1] J. Tolar, S.L. Teitelbaum, P.J. Orchard, Osteopetrosis, N Engl J Med 351(27) (2004) 2839-49.

[2] J. Bollerslev, Osteopetrosis. A genetic and epidemiological study, Clin Genet 31(2) (1987) 86-90.

[3] J. Bollerslev, K. Henriksen, M.F. Nielsen, K. Brixen, W. Van Hul, Autosomal dominant osteopetrosis revisited: lessons from recent studies, Eur J Endocrinol 169(2) (2013) R39-57.

[4] Z. Stark, R. Savarirayan, Osteopetrosis, Orphanet J Rare Dis 4 (2009) 5.

[5] A. Teti, M.J. Econs, Osteopetroses, emphasizing potential approaches to treatment, Bone (2017).

[6] L. Leisle, C.F. Ludwig, F.A. Wagner, T.J. Jentsch, T. Stauber, ClC-7 is a slowly voltage-gated 2Cl(-)/1H(+)-exchanger and requires Ostm1 for transport activity, EMBO J 30(11) (2011) 2140-52.

[7] A.R. Graves, P.K. Curran, C.L. Smith, J.A. Mindell, The Cl-/H+ antiporter ClC-7 is the primary chloride permeation pathway in lysosomes, Nature 453(7196) (2008) 788-92.

[8] C.F. Ludwig, F. Ullrich, L. Leisle, T. Stauber, T.J. Jentsch, Common gating of both CLC transporter subunits underlies voltage-dependent activation of the 2Cl-/1H+ exchanger ClC-7/Ostm1, J Biol Chem 288(40) (2013) 28611-9.

[9] E. Cleiren, O. Benichou, E. Van Hul, J. Gram, J. Bollerslev, F.R. Singer, K. Beaverson, A. Aledo, M.P. Whyte, T. Yoneyama, M.C. deVernejoul, W. Van Hul, Albers-Schonberg disease (autosomal dominant osteopetrosis, type II) results from mutations in the ClCN7 chloride channel gene, Hum Mol Genet 10(25) (2001) 2861-7.

[10] I. Alam, A.K. Gray, K. Chu, S. Ichikawa, K.S. Mohammad, M. Capannolo, M. Capulli, A. Maurizi, M. Muraca, A. Teti, M.J. Econs, A. Del Fattore, Generation of the first autosomal dominant osteopetrosis type II (ADO2) disease models, Bone 59 (2014) 66-75.

[11] S.G. Waguespack, S.L. Hui, L.A. Dimeglio, M.J. Econs, Autosomal dominant osteopetrosis: clinical severity and natural history of 94 subjects with a chloride channel 7 gene mutation, J Clin Endocrinol Metab 92(3) (2007) 771-8.

[12] I. Alam, A.K. McQueen, D. Acton, A.M. Reilly, R.L. Gerard-O'Riley, D.K. Oakes, C. Kasipathi, A. Huffer, W.B. Wright, M.J. Econs, Phenotypic severity of autosomal dominant osteopetrosis type II (ADO2) mice on different genetic backgrounds recapitulates the features of human disease, Bone 94 (2017) 34-41.

[13] L.L. Key, Jr., R.M. Rodriguiz, S.M. Willi, N.M. Wright, H.C. Hatcher, D.R. Eyre, J.K. Cure, P.P. Griffin, W.L. Ries, Long-term treatment of osteopetrosis with recombinant human interferon gamma, N Engl J Med 332(24) (1995) 1594-9.

[14] I. Alam, A.K. Gray, D. Acton, R.L. Gerard-O'Riley, A.M. Reilly, M.J. Econs, Interferon Gamma, but not Calcitriol Improves the Osteopetrotic Phenotypes in ADO2 Mice, J Bone Miner Res 30(11) (2015) 2005-13.

[15] S.J. Pettitt, Q. Liang, X.Y. Rairdan, J.L. Moran, H.M. Prosser, D.R. Beier, K.C. Lloyd, A. Bradley, W.C. Skarnes, Agouti C57BL/6N embryonic stem cells for mouse genetic resources, Nat Methods 6(7) (2009) 493-5.

[16] X. Mao, Y. Fujiwara, S.H. Orkin, Improved reporter strain for monitoring Cre recombinase-mediated DNA excisions in mice, Proc Natl Acad Sci U S A 96(9) (1999) 5037-42.

[17] G.E. Truett, P. Heeger, R.L. Mynatt, A.A. Truett, J.A. Walker, M.L. Warman, Preparation of PCR-quality mouse genomic DNA with hot sodium hydroxide and tris (HotSHOT), Biotechniques 29(1) (2000) 52, 54.

[18] C.M. Jacobsen, L.A. Barber, U.M. Ayturk, H.J. Roberts, L.E. Deal, M.A. Schwartz, M. Weis, D. Eyre, D. Zurakowski, A.G. Robling, M.L. Warman, Targeting the LRP5 pathway improves bone properties in a mouse model of osteogenesis imperfecta, J Bone Miner Res 29(10) (2014) 2297-306.

[19] Y. Cui, P.J. Niziolek, B.T. MacDonald, C.R. Zylstra, N. Alenina, D.R. Robinson, Z. Zhong, S. Matthes, C.M. Jacobsen, R.A. Conlon, R. Brommage, Q. Liu, F. Mseeh, D.R. Powell, Q.M. Yang, B. Zambrowicz, H. Gerrits, J.A. Gossen, X. He, M. Bader, B.O. Williams, M.L. Warman, A.G. Robling, Lrp5 functions in bone to regulate bone mass, Nat Med 17(6) (2011) 684-91.

[20] K. Sawakami, A.G. Robling, M. Ai, N.D. Pitner, D. Liu, S.J. Warden, J. Li, P. Maye, D.W. Rowe, R.L. Duncan, M.L. Warman, C.H. Turner, The Wnt co-receptor LRP5 is essential for skeletal mechanotransduction but not for the anabolic bone response to parathyroid hormone treatment, J Biol Chem 281(33) (2006) 23698-711.

[21] M.L. Bouxsein, S.K. Boyd, B.A. Christiansen, R.E. Guldberg, K.J. Jepsen, R. Muller, Guidelines for assessment of bone microstructure in rodents using micro-computed tomography, J Bone Miner Res 25(7) (2010) 1468-86.

[22] D.W. Dempster, J.E. Compston, M.K. Drezner, F.H. Glorieux, J.A. Kanis, H. Malluche, P.J. Meunier, S.M. Ott, R.R. Recker, A.M. Parfitt, Standardized nomenclature, symbols, and

units for bone histomorphometry: a 2012 update of the report of the ASBMR Histomorphometry Nomenclature Committee, J Bone Miner Res 28(1) (2013) 2-17.

[23] U. Kornak, D. Kasper, M.R. Bosl, E. Kaiser, M. Schweizer, A. Schulz, W. Friedrich, G. Delling, T.J. Jentsch, Loss of the ClC-7 chloride channel leads to osteopetrosis in mice and man, Cell 104(2) (2001) 205-15.

[24] B.P. Sinder, M.M. Eddy, M.S. Ominsky, M.S. Caird, J.C. Marini, K.M. Kozloff, Sclerostin antibody improves skeletal parameters in a Brtl/+ mouse model of osteogenesis imperfecta, J Bone Miner Res 28(1) (2013) 73-80.

[25] A. Sato, J. Ouellet, T. Muneta, F.H. Glorieux, F. Rauch, Scoliosis in osteogenesis imperfecta caused by COL1A1/COL1A2 mutations - genotype-phenotype correlations and effect of bisphosphonate treatment, Bone 86 (2016) 53-7.

[26] S.H. Rao, K.D. Evans, A.M. Oberbauer, R.B. Martin, Bisphosphonate treatment in the oim mouse model alters bone modeling during growth, J Biomech 41(16) (2008) 3371-6.

[27] E.S. Orwoll, J. Shapiro, S. Veith, Y. Wang, J. Lapidus, C. Vanek, J.L. Reeder, T.M. Keaveny, D.C. Lee, M.A. Mullins, S.C. Nagamani, B. Lee, Evaluation of teriparatide treatment in adults with osteogenesis imperfecta, J Clin Invest 124(2) (2014) 491-8.

[28] I. Grafe, S. Alexander, T. Yang, C. Lietman, E.P. Homan, E. Munivez, Y. Chen, M.M. Jiang, T. Bertin, B. Dawson, F. Asuncion, H.Z. Ke, M.S. Ominsky, B. Lee, Sclerostin Antibody Treatment Improves the Bone Phenotype of Crtap(-/-) Mice, a Model of Recessive Osteogenesis Imperfecta, J Bone Miner Res 31(5) (2016) 1030-40.

[29] T.E. Uveges, K.M. Kozloff, J.M. Ty, F. Ledgard, C.L. Raggio, G. Gronowicz, S.A. Goldstein, J.C. Marini, Alendronate treatment of the brtl osteogenesis imperfecta mouse improves femoral geometry and load response before fracture but decreases predicted material properties and has detrimental effects on osteoblasts and bone formation, J Bone Miner Res 24(5) (2009) 849-59.

[30] C.M. Jacobsen, M.A. Schwartz, H.J. Roberts, K.E. Lim, L. Spevak, A.L. Boskey, D. Zurakowski, A.G. Robling, M.L. Warman, Enhanced Wnt signaling improves bone mass and strength, but not brittleness, in the Col1a1(+/mov13) mouse model of type I Osteogenesis Imperfecta, Bone 90 (2016) 127-32.

[31] I. Fajac, K. De Boeck, New horizons for cystic fibrosis treatment, Pharmacol Ther 170 (2017) 205-211.

[32] J. Bollerslev, S.C. Marks, Jr., S. Pockwinse, M. Kassem, K. Brixen, T. Steiniche, L. Mosekilde, Ultrastructural investigations of bone resorptive cells in two types of autosomal dominant osteopetrosis, Bone 14(6) (1993) 865-9.

[33] P. Schulz, J. Werner, T. Stauber, K. Henriksen, K. Fendler, The G215R mutation in the Cl-/H+-antiporter ClC-7 found in ADO II osteopetrosis does not abolish function but causes a severe trafficking defect, PLoS One 5(9) (2010) e12585.

[34] J.R. Lees, Interferon gamma in autoimmunity: A complicated player on a complex stage, Cytokine 74(1) (2015) 18-26.

[35] D.Y. Kim, D.K. Han, H.J. Baek, S.T. Jung, H. Kook, T.J. Hwang, Long-term recombinant interferon-γ treatment in 2 cases of osteopetrosis, Korean J Pediatr 50(11) (2007) 1129-1133.

[36] P.R. Madyastha, S. Yang, W.L. Ries, L.L. Key, Jr., IFN-gamma enhances osteoclast generation in cultures of peripheral blood from osteopetrotic patients and normalizes superoxide production, J Interferon Cytokine Res 20(7) (2000) 645-52.

[37] S. Kamolmatyakul, W. Chen, Y.P. Li, Interferon-gamma down-regulates gene expression of cathepsin K in osteoclasts and inhibits osteoclast formation, J Dent Res 80(1) (2001) 351-5.

[38] S. Huang, W. Hendriks, A. Althage, S. Hemmi, H. Bluethmann, R. Kamijo, J. Vilcek, R.M. Zinkernagel, M. Aguet, Immune response in mice that lack the interferon-gamma receptor, Science 259(5102) (1993) 1742-5.

[39] G. Duque, D.C. Huang, N. Dion, M. Macoritto, D. Rivas, W. Li, X.F. Yang, J. Li, J. Lian, F.T. Marino, J. Barralet, V. Lascau, C. Deschenes, L.G. Ste-Marie, R. Kremer, Interferon-gamma plays a role in bone formation in vivo and rescues osteoporosis in ovariectomized mice, J Bone Miner Res 26(7) (2011) 1472-83.

[40] J. Bollerslev, T. Steiniche, F. Melsen, L. Mosekilde, Structural and histomorphometric studies of iliac crest trabecular and cortical bone in autosomal dominant osteopetrosis: a study of two radiological types, Bone 10(1) (1989) 19-24.

Figure legends

Figure 1. Generation of mice with a *Clcn7*^{F318L} knockin allele that is expressed and translated into protein.

(A) Schematic depiction of the wildtype (wt) *Clcn7* locus and the gene targeting construct (not drawn to scale) indicating the locations of PCR primers used to amplify DNA for the homologous recombination arms within the targeting vector (P1-P4) and to confirm correct targeting of the locus (P5-P8). The targeting construct includes a neomycin resistance cassette (Neo^{R}) flanked by loxP sites for positive selection, the p.F318L mutation in exon 11 (*), and a thymidine kinase (TK) cassette for negative selection. After achieving germline transmission, the Neo^{R} cassette was removed by Cre-recombination. The bottom schematic depicts the mutant *Clcn7* locus used in all animal experiments, with the location of primers (P9 and P10) used for genotyping indicated. (B) Representative image of a genotyping gel showing a 407 bp wildtype amplimer and a 530 bp mutant amplimer. (C) Sequencing electropherogram of PCR amplimer generated from a *Clcn7*$^{F318L/+}$ mouse confirming heterozygosity for the T→C transition. (D) RT-PCR using RNA from *Clcn7*$^{+/+}$, *Clcn7*$^{F318L/+}$ and *Clcn7*$^{F318L/F318L}$ tibial bone showing the expected 677 bp amplimer in each sample, with no evidence of altered splicing due to the *Clcn7*^{F318L} allele. (E) Bar graph depicting droplet digital PCR results using cDNA from *Clcn7*$^{+/+}$, *Clcn7*$^{F318L/+}$ and *Clcn7*$^{F318L/F318L}$ tibial bone showing the percentage of droplets than contain mutant or wildtype amplimers. Samples from 3 mice with each genotype were studied, and ddPCR reactions were performed in duplicate. An average of 163 amplimer containing droplets were detected per reaction. (F) Fluorescence photomicrographs of cultured bone marrow cells isolated from *Clcn7*$^{+/+}$ and *Clcn7*$^{F318L/F318L}$ mice that had been incubated with an anti-CLC-7 primary antibody and a FITC-labeled (green fluorescence) secondary antibody. Nuclei were stained with Hoechst 33342 dye and

fluoresce blue. Note *Clcn7*$^{+/+}$ and *Clcn7*$^{F318L/F318L}$ cells have similar patterns of CLC-7 immunofluorescence. Importantly, in the absence of primary antibody, these immunofluorescence signals were not observed in these cells (data not shown). Scale bar equals 10 μm.

Figure 2. Twelve-week-old *Clcn7*$^{F318L/+}$ mice have a skeletal phenotype.

(A) Bar graphs indicating the mean (±1SD) weight, bone mineral density (BMD), and bone mineral content (BMC) of 12-week-old female and male *Clcn7*$^{+/+}$ (wt) and *Clcn7*$^{F318L/+}$ (het) mice. (B) Representative reconstructed microCT cross sectional images of midshaft and distal femur, and coronal images of the distal femur in wt and het mice. Bar graphs indicating mean (±1SD) values for wt and het mouse trabecular bone volume fraction (BV/TV), trabecular number (Tb.N), trabecular thickness (Tb.Th), trabecular separation (Tb.Sp), cortical area fraction (Ct.Ar/Tt.Ar) and cortical thickness (Ct.Th). Note that trabecular bone values are significantly affected by the *Clcn7*^{F318L} allele, whereas cortical bone values are only affected in males. (C) Bar graphs indicating mean (±1SD) biomechanical values for female and male wt and het mouse femurs measured during three-point bending. The *Clcn7*^{F318L} allele was not associated with significant differences in any measured value in females, however, males showed a decrease in energy to ultimate force. In all panels, values above the graphs are ANOVA and Bonferroni corrected p values, and values below the graphs indicate the number of animals studied in each cohort.

Figure 3. A skeletal phenotype is detectable in 3-week-old *Clcn7*$^{F318L/F318L}$ mice, but not in *Clcn7*$^{F318L/+}$ mice.

(A) Bar graphs indicating the mean (±1SD) weight and bone mineral density (BMD) in 3-week-old female and male *Clcn7*$^{+/+}$ (wt), *Clcn7*$^{F318L/+}$ (het), and *Clcn7*$^{F318L/F318L}$ (hom) mice. *

above the bars represent significant p values for wt vs. hom and het vs. hom comparisons calculated using ANOVA and Bonferroni correction, and values below the graphs indicate the number of animals studied in each cohort. (B) Representative reconstructed μCT cross sectional images of midshaft and distal femur, and coronal images of the entire femur in wt, het, and hom mice.

Figure 4. IFN-G does not improve bone properties in *Clcn7*$^{F318L/+}$ mice.

Bar graphs indicating the mean (±1SD) weight, bone mineral density (BMD), and trabecular bone volume fraction (BV/TV) by μCT of 12-week-old female and male *Clcn7*$^{+/+}$ (wt) and *Clcn7*$^{F318L/+}$ (het) mice that received vehicle (-) or IFN-G (+) from 4 to 12 weeks of age. As previously observed (see Figure 2) BV/TV is significantly increased in het compared to wt mice. However, IFN-G treatment did not affect BV/TV in mice with either genotype. Values below the graphs indicate the number of animals studied in each cohort.

Figure 5. IFN-G decreases osteoclast surface and bone turnover in *Clcn7*$^{F318L/+}$ mice.

(A) Representative photomicrographs of bone sections stained for TRAP from 12-week-old male *Clcn7*$^{+/+}$ (wt) and *Clcn7*$^{F318L/+}$ (het) mice that received vehicle (-) or IFN-G (+) from 4 to 12 weeks of age. (B) Bar graphs indicating mean (±1SD) values for number of osteoclast per bone perimeter (N.Oc/B.Pm), osteoclast surface (N.Oc/BS), number of osteoblast per bone perimeter (N.Ob/B.Pm) and osteoblast surface (N.Ob/BS) in wt and het male mice. Note that osteoclast parameters are significantly affected by the *Clcn7*^{F318L} allele and normalize with treatment with IFN-G. (C) Representative photomicrographs of dual fluorochrome (calcein and alizarin red complexome) labeled distal femur metaphysis from 12-week-old male wt and het mice that received vehicle (-) or IFN-G (+) from 4 to 12 weeks of age. (D) Bar graphs indicating mean (±1SD) values for mineralizing surface (MS/BS), mineral apposition rate

(MAR), bone formation rate (BFR/BS) and bone turnover rate (BFR/BV) in wt and het male mice. Note that MS/BS, MAR and BFR/BV are affected by IFN-G treatment, which can be appreciated in the photomicrographs (distance between the red and green labels in the close-up panels). The increase in trabecular bone fraction among het mice is also visible. (E) Bar graphs depicting the mean (±1SD) serum values of procollagen type 1 N terminal propeptide (P1NP), an indicator of bone anabolism, tartrate resistant acid phosphatase 5b (TRAcP 5b), an indicator of osteoclast number, and C terminal telopeptide of type 1 collagen (CTX-I), an indicator of osteoclast mediated bone catabolism. Only TRAcP 5b levels were significantly increased in both male and female het mice compared to sex-matched wt mice, and significantly reduced in het mice that received IFN-G. However, IFN-G treatment did not significantly affect the bone catabolic marker CTX-I or the bone anabolic marker P1NP in both males and females. In all panels, values above the graphs are ANOVA and Bonferroni corrected p values, and values below the graphs indicate the number of animals studied in each cohort.

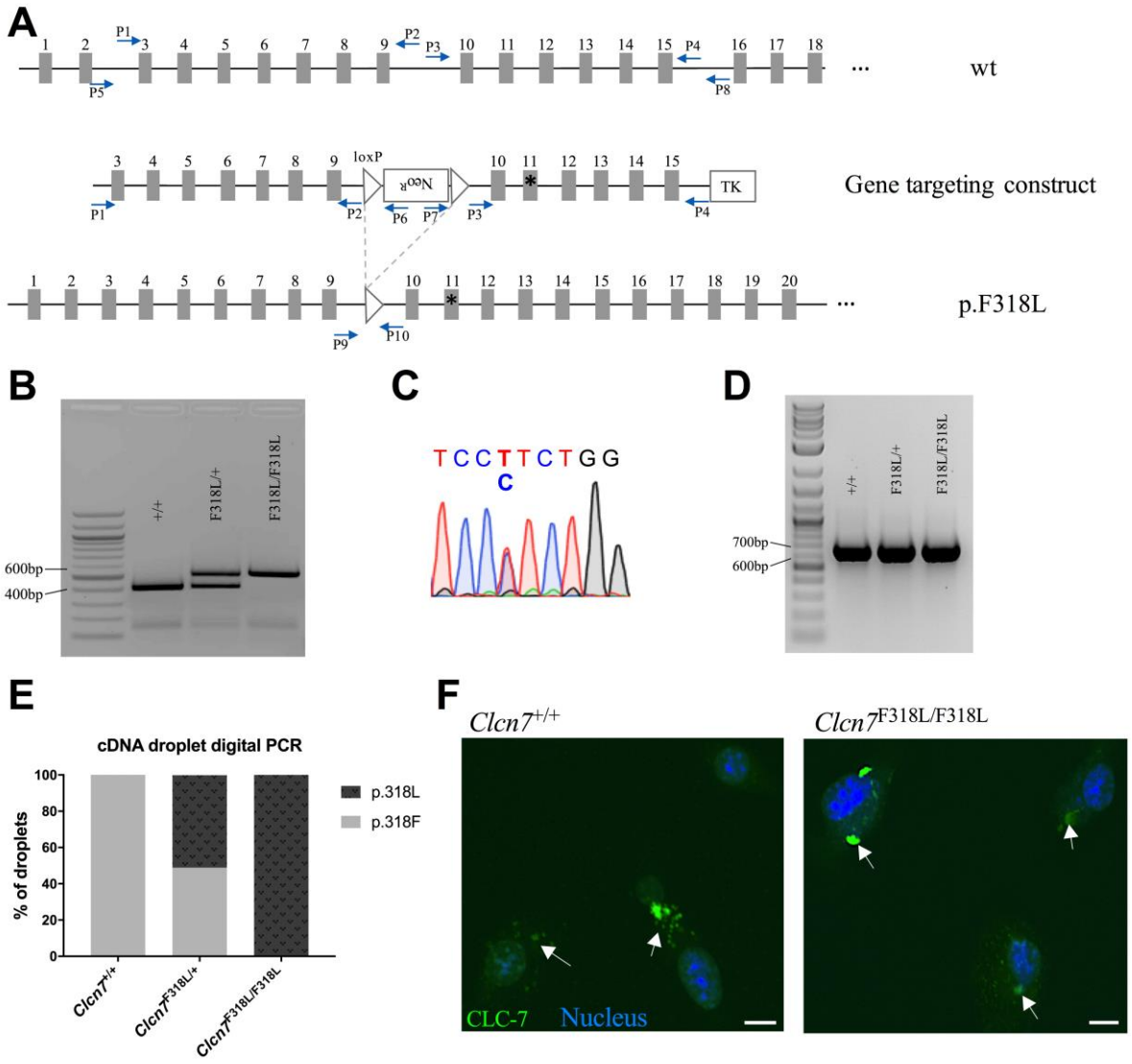

Fig. 1

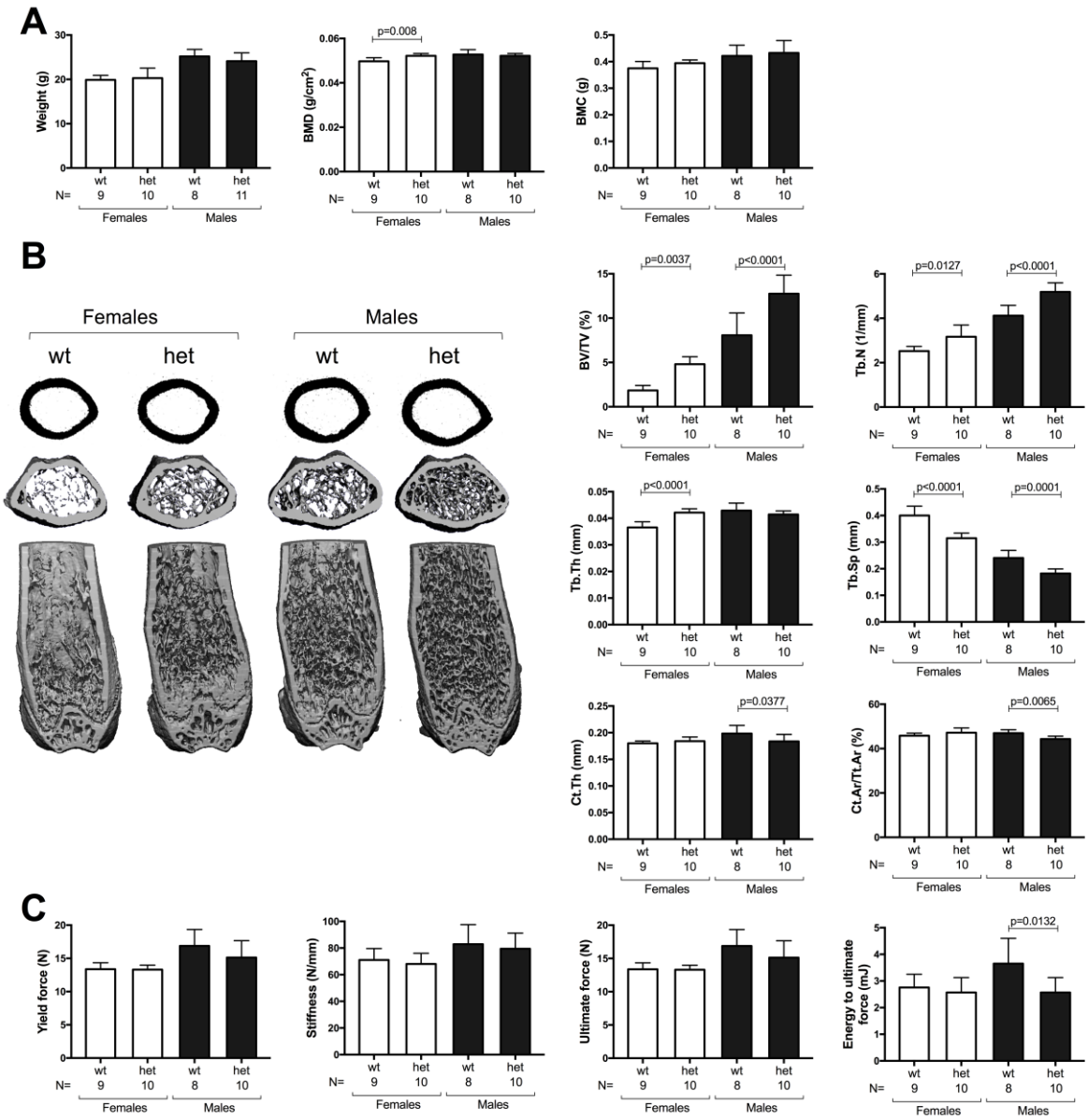

Fig. 2

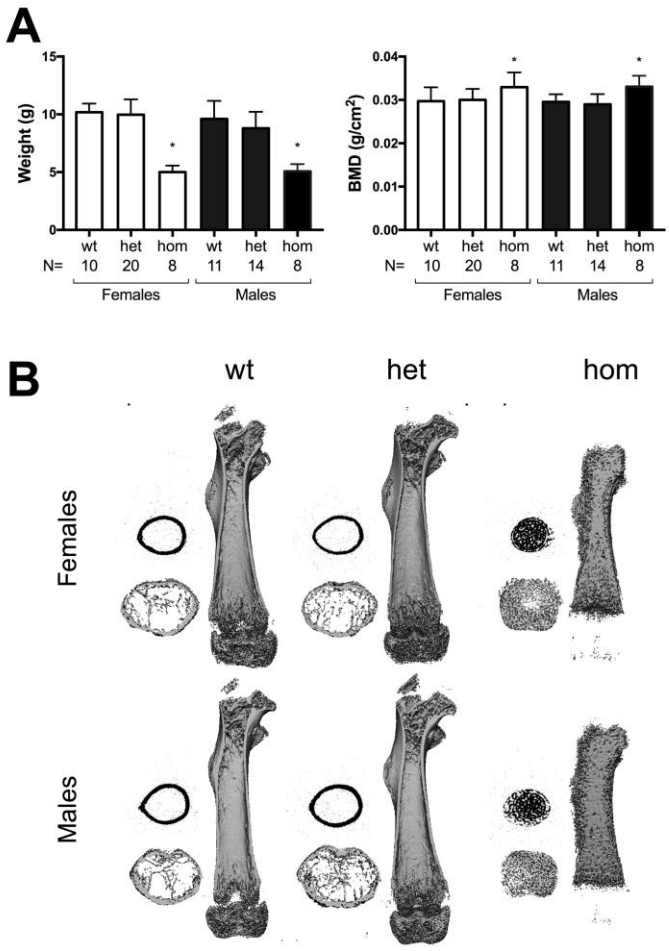

Fig. 3

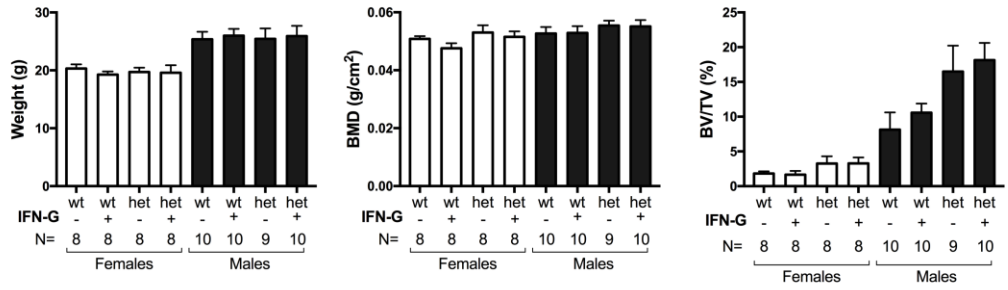

Fig. 4

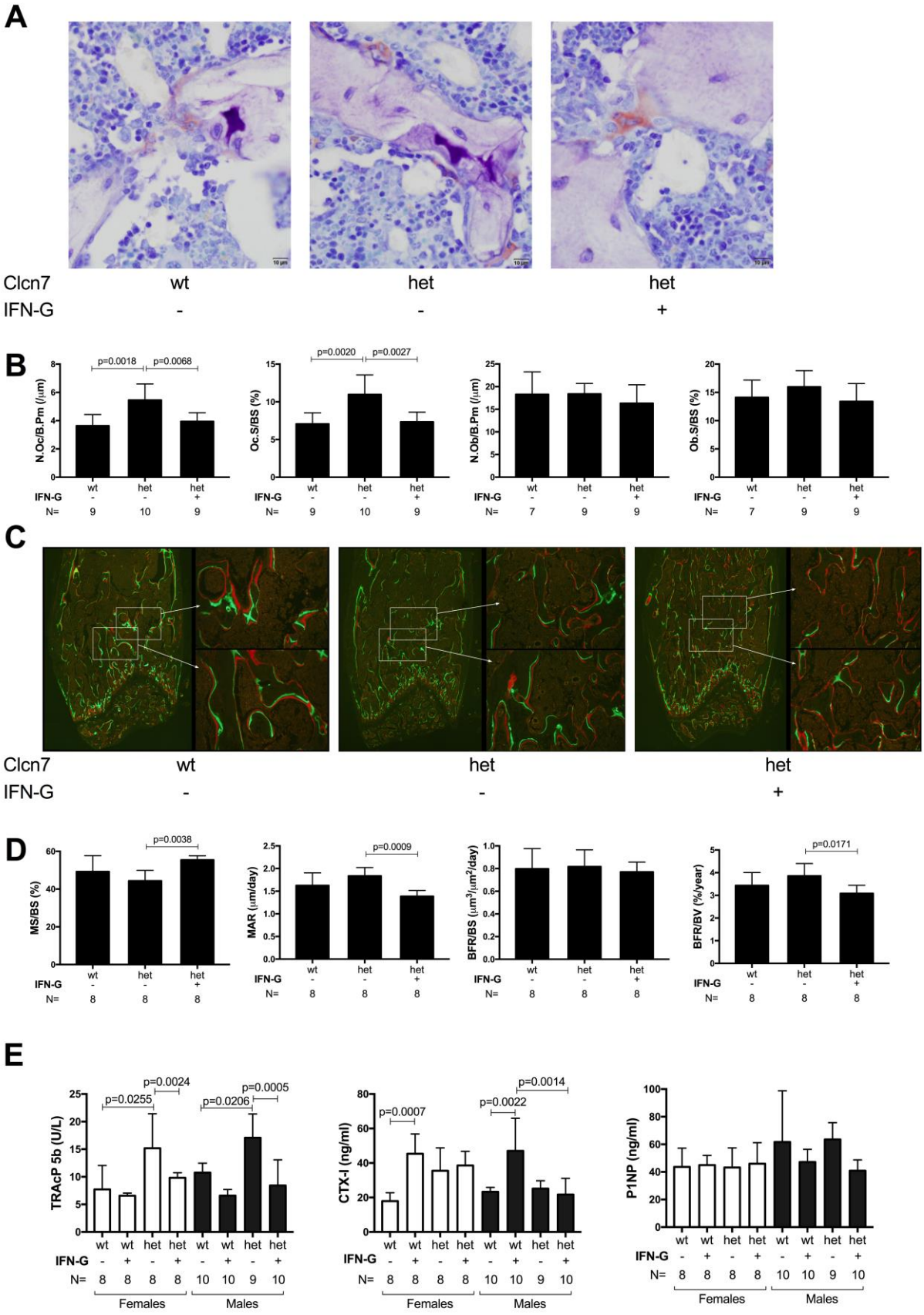
A
Clcn7 wt het het
IFN-G - - +
B
N.Oc/B.Pm (μm)
p=0.0018
p=0.0068
Oc.S/BS (%)
p=0.0020
p=0.0027
N.Ob/B.Pm (μm)
Ob.S/BS (%)
IFN-G wt het het
N= 9 10 9
N= 7 9 9
C
Clcn7 wt het het
IFN-G - - +
D
MS/BS (%)
p=0.0038
MAR (μm/day)
p=0.0009
BFR/BS (μm³/μm²/day)
BFR/BV (%/year)
p=0.0171
IFN-G wt het het
N= 8 8 8
E
TRAcP 5b (U/L)
p=0.0255
p=0.0024
p=0.0206
p=0.0005
CTX-I (ng/ml)
p=0.0007
p=0.0022
p=0.0014
P1NP (ng/ml)
IFN-G wt wt het het wt wt het het
- + - + - + - +
N= 8 8 8 8 10 10 9 10
Females
Males

Fig. 5

Highlights

- A new model of Albers-Schönberg disease has been created with *Clcn7*$^{F318L/+}$ mice.
- *Clcn7*$^{F318L/+}$ mice have increased numbers of osteoclasts and increased trabecular bone volume when compared to *Clcn7*$^{+/+}$ littermates.
- Interferon-gamma treatment of *Clcn7*$^{F318L/+}$ mice normalized the number of osteoclasts, but had no effect on trabecular bone volume.